Hindawi
Advances in Meteorology
Volume 2017, Article ID 2764340, 18 pages
https://doi.org/10.1155/2017/2764340

Research Article

Observational and Simulative Study of a Local Severe Precipitation Event Caused by a Cold Vortex over Northeast China

Ying Liu,[1] Zhaoming Liang,[1] and Yupeng Li[2]

[1]*State Key Laboratory of Severe Weather, Chinese Academy of Meteorological Sciences, Beijing 100081, China*
[2]*Jilin Research Institute of Meteorological Science, Changchun 130062, China*

Correspondence should be addressed to Ying Liu; y119@camscma.cn

Received 22 June 2017; Revised 19 September 2017; Accepted 25 September 2017; Published 5 December 2017

Academic Editor: Anthony R. Lupo

A severe precipitation event around Changchun-Yongji in Jilin Province, China, during 27–29 July 2010 was investigated, with a focus on the comparative analysis of 2 heavy precipitation episodes. This was done using NCEP gridded analysis data, intensive surface observations, and radar and satellite measurements. The Weather Research and Forecast (WRF) model was used to simulate the precipitation process and explore mechanisms for the development and dissipation of the severe precipitation event. Precipitation in the first stage was induced by the convergence of northwesterly winds at the rear of the cold vortex and southwesterly winds that reached the rainfall region. However, in the second stage, because of the blockage caused by Changbai Mountain, winds at the bottom of the cold vortex turned from the northwest to the northeast. These winds strongly converged with the southwesterly winds and continuously triggered new convective clouds, which were associated with cold centers at the surface. The intensity of the cold center modulated the strength of the convective cells and resulting precipitation quantity. Furthermore, the local terrain features and direction of the motion of the airflows were critical in triggering convection.

1. Introduction

A cutoff low (COL) is a closed upper-tropospheric low-pressure system that is completely detached (cut off) from its polar source and extends to the south of the mid-latitude westerly mean flow as a result of the deepening of a high-level trough [1, 2]. In China, a COL is traditionally called a northeast cold vortex. The northeast cold vortex is an important component of atmospheric circulation and a critical weather system in Northeast China. It can occur over 35°–60°N and 115°–145°E [3] almost year-round but mainly occurs in the summer [4]. Not only is the vortex an important weather system that affects precipitation in Northeast China [5, 6], but also it can induce the southward migration of cold air masses that affect the Jianghuai region [7] and southern China [8]. The vortex can often induce abrupt and strong convective weather systems that produce heavy rainfall, thunderstorms, hail, and other catastrophic weather events [9, 10]. Local severe convective weather events induced by the northeast cold vortex have always been an important but difficult issue in operational weather forecasting.

In recent years, most frequent, strong convective weather events (e.g., squall lines) were associated with the northeast cold vortex.

A strong squall line accompanied by disastrously strong surface winds occurred over Henan Province from around noon on 3 June to early morning of 4 June 2009. Strong winds exceeding 17 m s^{-1} were observed in 19 counties, and a maximum speed of 29 m s^{-1} (the 11th scale) was measured at 22:42 LST at Yongcheng in Shangqiu. This was the strongest measurement on record in this location since 1957, when weather data first became available. This occurrence resulted in 18 deaths and 81 injuries. Liu and Guo [11] investigated the mechanisms for the formation and structure of this squall line. They found that it was formed mainly under the influence of the northeast cold vortex. A cold air mass was steered by an inverted trough to the rear of the northeast cold vortex, which moved southwards and converged with

warm, moist southwesterly winds over Xinxiang in Henan. This triggered the strong convection that eventually evolved into a squall line.

Statistical analysis has suggested that most severe convective weather events in eastern China from April through June are related to the northeast cold vortex [12]. On 5 June 2009, hail 25–30 mm in diameter occurred over parts of Shanghai due to the influence of a single supercell thunderstorm in advance of the squall line. The squall line later moved across Shanghai behind this thunderstorm and produced strong winds, lightning, and heavy precipitation. Dai et al. [13] indicated that this thunderstorm formed under a strongly unstable stratification caused by a strong cold advection southwest of the northeast cold vortex at the upper levels and warm advection at the lower levels. The inverted trough to the southwest of the northeast cold vortex moved southwards, which led to colder temperatures, and the heights of the 0°C and −20°C levels decreased significantly. This provided a more favorable temperature environment for the growth of hail. The lower 0°C level ensured that hail would not melt much during its descent.

The cold vortex at high altitudes is a deep, convergent weather system that can persist for 3–6 days. In 1949, Hsieh [14] investigated a cold vortex over North America and provided a detailed description of the formation and evolution of the cold vortex; he also found the indirect circulation involved in the cold vortex. The cold air mass steered by the strong northwesterly flows to the southwest of a cold vortex can trigger convective systems in middle and low latitudes. In recent years, many researchers have investigated severe convective weather events at the middle and low latitudes, which are initiated by the southward movement of a cold air mass steered by the northeast cold vortex [14–18]. Their results indicated that convective weather events accompanied by a cold vortex are often characterized by their small scale, abrupt occurrence, complicated weather phenomena, and great destructive potential. The synoptic weather pattern often shows strong northwesterly winds that are difficult to predict by either operational weather forecasts or numerical prediction.

A number of studies have investigated severe convection induced by the northeast cold vortex within that vortex or over mid- and high-latitude regions. For example, severe convective weather lasting 4 consecutive days affected 3 provinces in Northeast China during 9–12 July 2005. This is a typical feature of the northeast cold vortex, which often generates continuous, severe convection over its area of influence. Chen et al. [19] analyzed the environmental characteristics of this weather event. Li et al. [20] investigated a locally heavy rainstorm over Shenyang and its vicinity, indicating that the cold vortex developed fully during this event and affected a large area. The primary rain area was not in Northeast China. Instead, the area extended from the Shandong Peninsula (including Qin Huang Dao) across the Yangtze River valley to the northeastern part of southwest China, where the cold air mass encountered a warm air mass from the south. At 16:00 UTC (all times in this manuscript are given in UTC), 10 August 2005, a short-lived tornado occurred in southeastern Yingkou, causing casualties and significant economic losses [21]. From 19 July to the end of August 2010, there were 10 consecutive precipitation events in Jilin and Liaoning. Both the frequency and intensity of the precipitation processes involved were historically rare. Sun et al. [22] analyzed those processes and discovered that 7 out of 10 were produced by the eastward movement of the northeast cold vortex. Rain clouds continued forming and traversing the same area, leading to heavy accumulated precipitation.

The above brief review indicates that severe convective weather caused by the northeast cold vortex may occur in various areas, with complex weather events occurring frequently under a complicated background synoptic pattern. This poses a great challenge to practical weather forecasts. Many researchers have investigated the mechanisms for mesoscale systems induced by the vortex and the evolution of these systems; their focus was on the forecasting problems of severe convective weather accompanied by the northeast cold vortex. These studies were attempted to better understand the structure of the vortex, the mechanism for the generation and development of the aforementioned mesoscale systems, and the structures of those systems within the vortex, with the aim of ultimately improving the overall forecast of severe convective weather events associated with the vortex. However, given the limitations of the observations and research tools, most of the studies focused on the climatic features, synoptic weather patterns, and diagnostic analysis of synoptic settings for the development of the mesoscale systems. Mechanistic studies on the development of these systems are still inadequate.

A well-known, large-scale rainstorm event occurred over central-eastern Jilin on 2 consecutive days, during 27–29 July 2010. Sun et al. [22] and Wang and Zhang [23] investigated this event from the perspectives of weather processes and forecasting techniques, respectively. They found that the rainstorm center covered Sanjiazi and Guanting, where the temporal variation in the hourly precipitation displayed a dual-peak feature, suggesting that the mesoscale rain clusters underwent intensification. In the present study, we utilized dense surface observations, radar and satellite measurements, NCAR/NCEP gridded analysis data (with a horizontal resolution of 0.5°× 0.5°), and numerical studies using the Weather Research and Forecasting Advanced Research (WRF-ARW) model to investigate the rainstorm process, with a focus on the mechanisms of rainstorm intensification. The objective was to reveal the triggering mechanisms and influences of the mesoscale system, specifically the dynamic mechanisms for the abrupt increases in the precipitation following a short break, thereby providing new insights into operational forecasting.

2. Large-Scale Circulation Background

Large-scale rainstorms occurred over central-eastern Jilin on 2 consecutive days, during 27–29 July 2010, with a severe precipitation event that occurred during the night of 27 July through the afternoon of 28 July. The rain belt extended west to east along Changchun, Yongji, Dunhua, and Yanji. From 12:00 on the 27th to 12:00 on the 28th, the 24 h accumulated precipitation (figure not shown) reached 243.1 mm

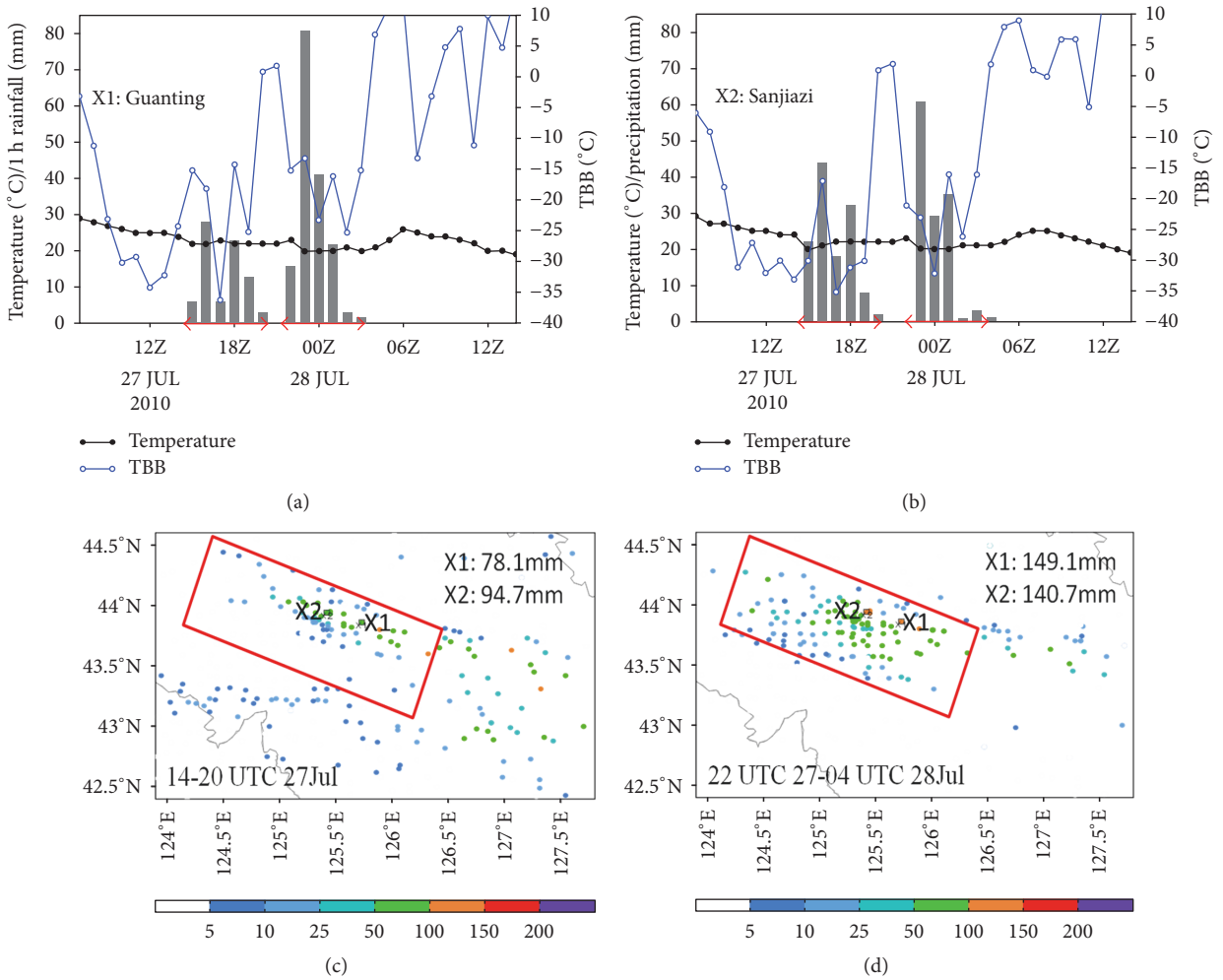

FIGURE 1: Hourly precipitation at Guanting (X1, a) and Sanjiazi (X2, b) (histogram, mm), TBB (blue curve, °C), and surface temperature (black curve, °C) from 06:00 on the 27th to 14:00 on the 28th. The 6 h accumulated precipitation during 2 periods of precipitation (colored dots, mm) are shown for (c) 14:00–20:00 on the 27th and (d) 22:00 on the 27th to 04:00 on the 28th.

and 252.5 mm at Guanting and Sanjiazi in Yongji County, respectively. The time series of the hourly precipitation shown in Figures 1(a) and 1(b) indicate that the precipitation was concentrated in 2 periods, 14:00–20:00 on the 27th and 22:00 on the 27th through 04:00 on the 28th. During the first stage, the hourly precipitation peak of 43 mm occurred at 16:00 on the 27th and, during the second stage, a peak of 80.5 mm occurred at 23:00 on the 27th. The 6 h accumulated precipitation reached 78.1 mm and 94.7 mm at Guanting and Sanjiazi, respectively (Figure 1(c)), during the first stage. The corresponding maxima in the second stage were 149.1 mm and 140.7 mm, respectively, much greater than those in the first stage (Figure 1(d)). Figures 1(c) and 1(d) also show the 2 rain belts during the first stage, in the north and south, with the precipitation in the southern belt being weaker than that in the north. In the second stage, the precipitation mainly occurred in the northern rain belt, which encompassed a larger rainfall area and greater intensity than in the first stage; the rain belt in the south had disappeared. There was a heavy rainstorm over most of central-eastern Jilin from 27 to 29 July. Statistical results indicated a record breaking 48 h accumulated precipitation during 08:00 on the 27th through 08:00 on the 29th at Huinan station, while the second heaviest precipitation was recorded at Yongji and Antu [23].

Figure 2 shows the 950 hPa circulation and precipitable water content at various times. At 12:00 on the 27th (Figure 2(a)), most of Jilin was under the influence of southwesterly winds. A high-temperature, high-moisture, low-level jet was southwest of the heavy rainstorm area, where the maximum precipitable water was >65 kg m^{-2}. There was a shear line southwest of the rain area. A warm center formed in northeastern Jilin under the influence of the warm, moist southwesterlies. At 18:00 (Figure 2(b)), the shear line intensified and moved east-northeastwards, reaching the heavy rain area. Areas with precipitable water >50 kg m^{-2} also moved east-northeastwards to reach the rainfall area. At 00:00 on the 28th, the shear line began to move eastwards, and northeasterly winds prevailed to the north of the line. The evolution of the radar reflectivity (shown later) showed that the cloud clusters affecting the rain area gradually moved southwest to northeast during the first stage and then west to

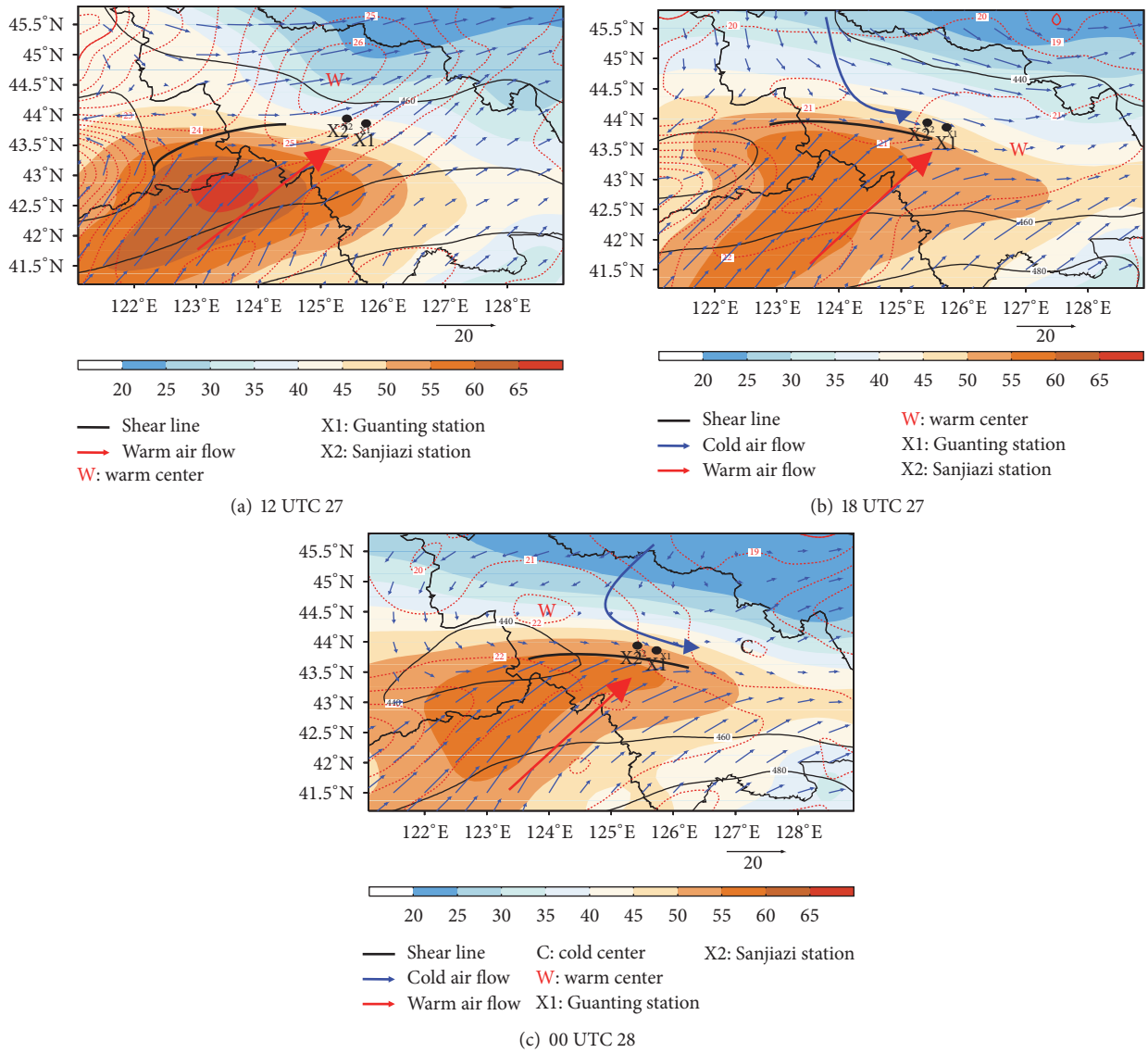

Figure 2: Geopotential height (black solid contours, geopotential decameters), temperature (red dashed contours, °C), wind vectors at 950 hPa, and precipitable water content (shaded, kg m^{-2}) at 12:00 on the 27th, (b) 18:00 on the 27th, and (c) 00:00 on the 28th.

east during the later stage, consistent with the evolution of a low-level shear line.

Figure 3 shows the 500 hPa geopotential height and temperature fields and 850 hPa relative humidity and wind fields. At 12:00 on 27 July, prior to the start of the heavy rain, central-western Jilin was at the bottom part of the cold vortex, and westerly winds prevailed over this region. At 850 hPa, water vapor was concentrated to the west of Changbai Mountain, with large values over Liaoning and eastern Jilin. As the cold vortex moved eastwards gradually and slowly, the northwesterlies at the bottom of the vortex were replaced by northerlies at 00:00 on the 28th. Concurrently, the southwesterly winds further intensified and moved northward, converging with the northwesterly winds at Jilin. An east–west shear line formed and severe precipitation developed.

Further analysis of the 500 hPa circulation pattern (Figure 4) suggests that the northwesterly winds prevailed in the rain area from 12:00 on the 27th to 00:00 on the 28th. However, the spatial pattern of the temperature indicated a cold center to the northwest of the rain area (near X1 and X2), suggesting that a strong cold advection to the rear of the rain area at upper levels corresponded to a warm center and warm advection at lower levels. Such a pattern intensified the instability and provided potential energy for the subsequent heavy rainstorm. The distribution of convective available potential energy (CAPE) indicates that the central rain area was at the edge of a large CAPE area. At 18:00 on the 27th (Figure 4(b)), temperatures changed substantially. A cold air mass invaded from the northeast of the rain area and advanced to the southwest, forming a low-temperature trough that extended northeast to southwest, which then

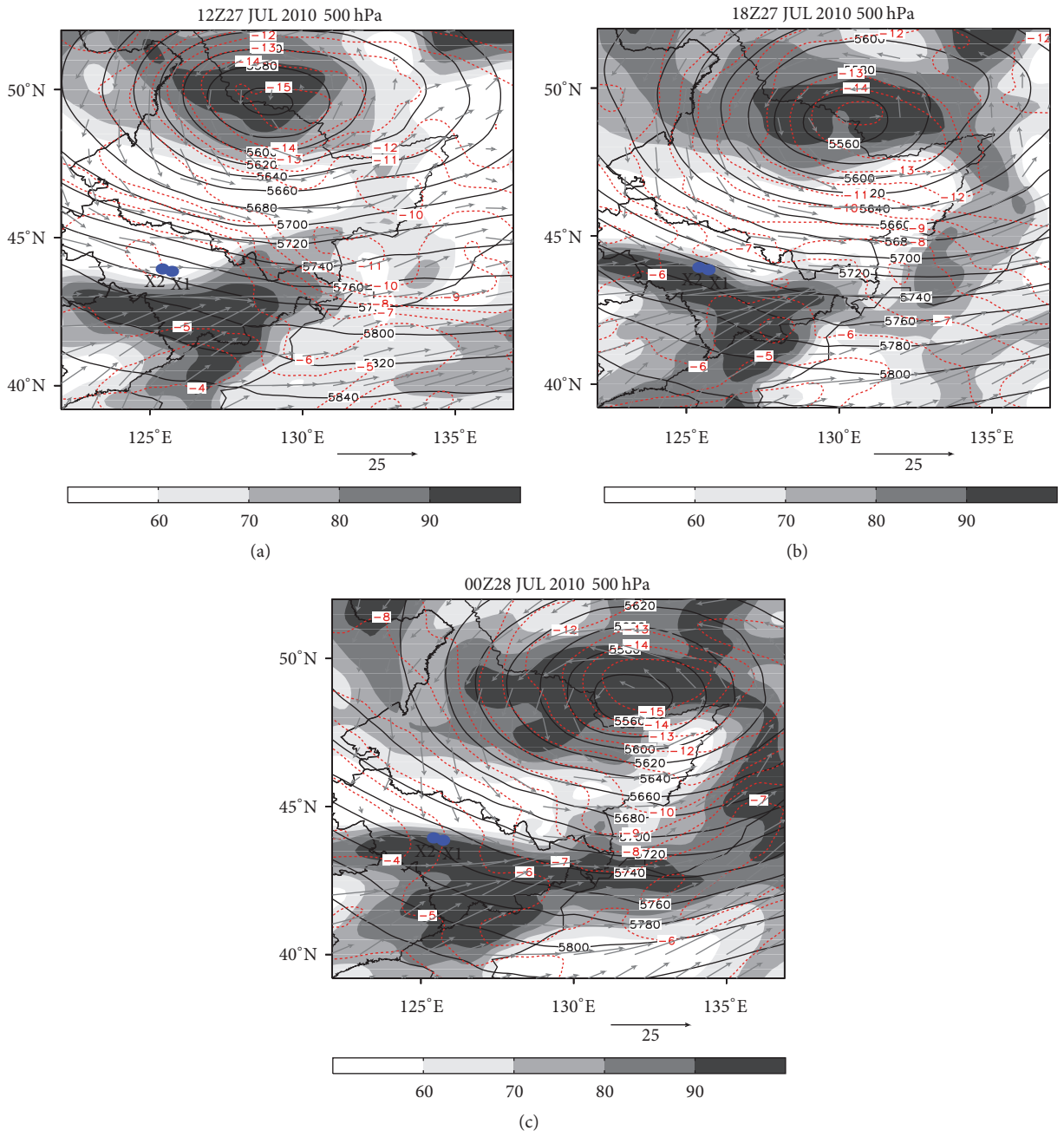

Figure 3: Geopotential height (black solid contours, gpm) and temperature (red dashed contours, °C) at 500 hPa and relative humidity (shaded, %) and wind vectors (m s^{-1}) at 850 hPa. X1 and X2 are the same as in Figure 1: (a) 12:00 on the 27th, (b) 18:00 on the 27th, and (c) 00:00 on the 28th.

gradually moved southeastwards. The invasion of this cold air mass was closely linked to the development of the rainstorm.

In the following section, we discuss the explanation for the precipitation intensification over Changchun and Yongji based on the NCEP gridded analysis data (with a horizontal resolution of 0.5°), Fengyun-2E satellite (FY2E) brightness temperatures and infrared imagery of clouds, and radar and surface intense observations. The infrared imagery indicated that rainfall in the second period was caused by newly generated cloud clusters in the mesoscale system. Thus, we focus on the analysis of the structure of the mesoscale cloud clusters and the possible mechanisms for their development.

3. Evolution of the Mesoscale Convective System

3.1. Evolution of Cloud Clusters. The time series of the hourly precipitation and brightness temperature (TBB) shown in Figure 1(a) suggests that the intensified precipitation from northern Changchun to Yongji was caused by newly

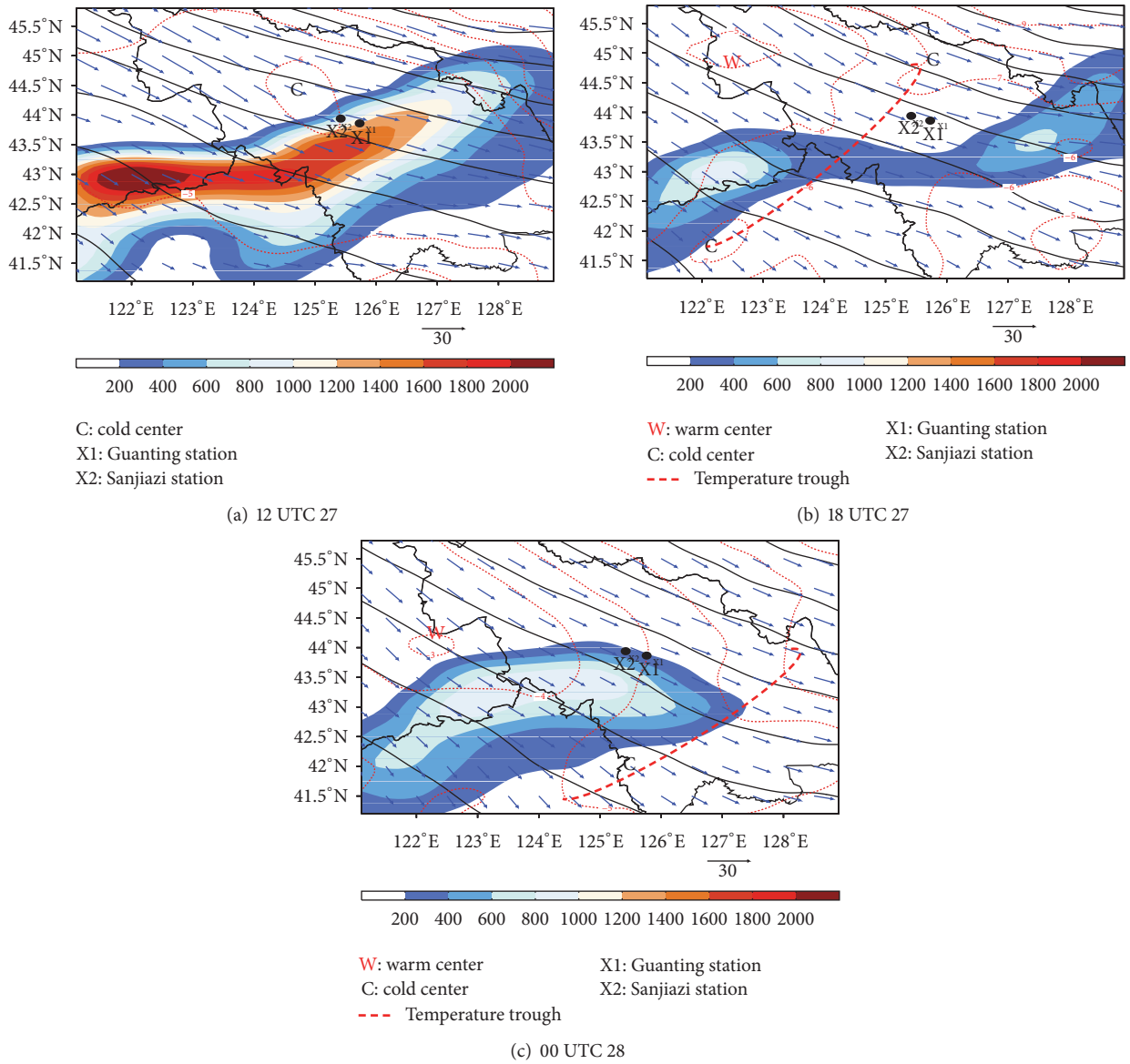

Figure 4: Geopotential height (black solid contours, gpm) and temperature (red dashed contours, °C) at 500 hPa and wind (vectors) and convective available potential energy (shaded, J kg^{-1}) at (a) 12:00 on the 27th, (b) 18:00 on the 27th, and (c) 00:00 on the 28th.

generated cloud clusters. Figure 5 shows the FY2E infrared images of clouds from 21:00 on the 27th to 00:00 on the 28th at half-hour intervals. At 21:00 on the 27th, multiple convective cloud cells (in a gray color) formed at the rear of the cold vortex. By 22:00, these cells merged and the cloud TBB brightened, suggesting that the cloud layers had become thicker with a higher cloud top height. A convective cloud belt of around 300 km in length formed from west to east and contained multiple convective cell centers. After 23:00, the newly formed cloud belt merged with clouds associated with the cold vortex and gradually moved southeastwards, with the rain belt motion following that of the cloud system.

Figure 6 displays the hourly TBB and precipitation at various times. At 20:00 on the 27th, the rain clouds that modulated the precipitation at Changchun and Yongji had moved to Yanji, while new isolated cloud clusters (C1 in the figure) formed at their rear. At 22:00 on the 27th, new cloud clusters formed to the west of C1, and the temperature at the cloud center decreased to −32°C. However, no closed isothermal lines could be found in the area from Guanting to Sanjiazi at this time (between X1 and X2 in the figure), but the hourly precipitation reached 17 mm. This implies that the influential system at this time was of a small scale and could not be resolved by the 10 km resolution TBB data. Only weak isolated convective cells could be detected from the infrared images of clouds. At 23:00, clouds with a temperature of −20°C extended west–east with a length of ~60 km between X1 and X2. A meso-γ-scale system with a temperature of −32°C developed along the northern flank of the clouds. The rapid formation and development of this cloud system directly resulted in the hourly precipitation

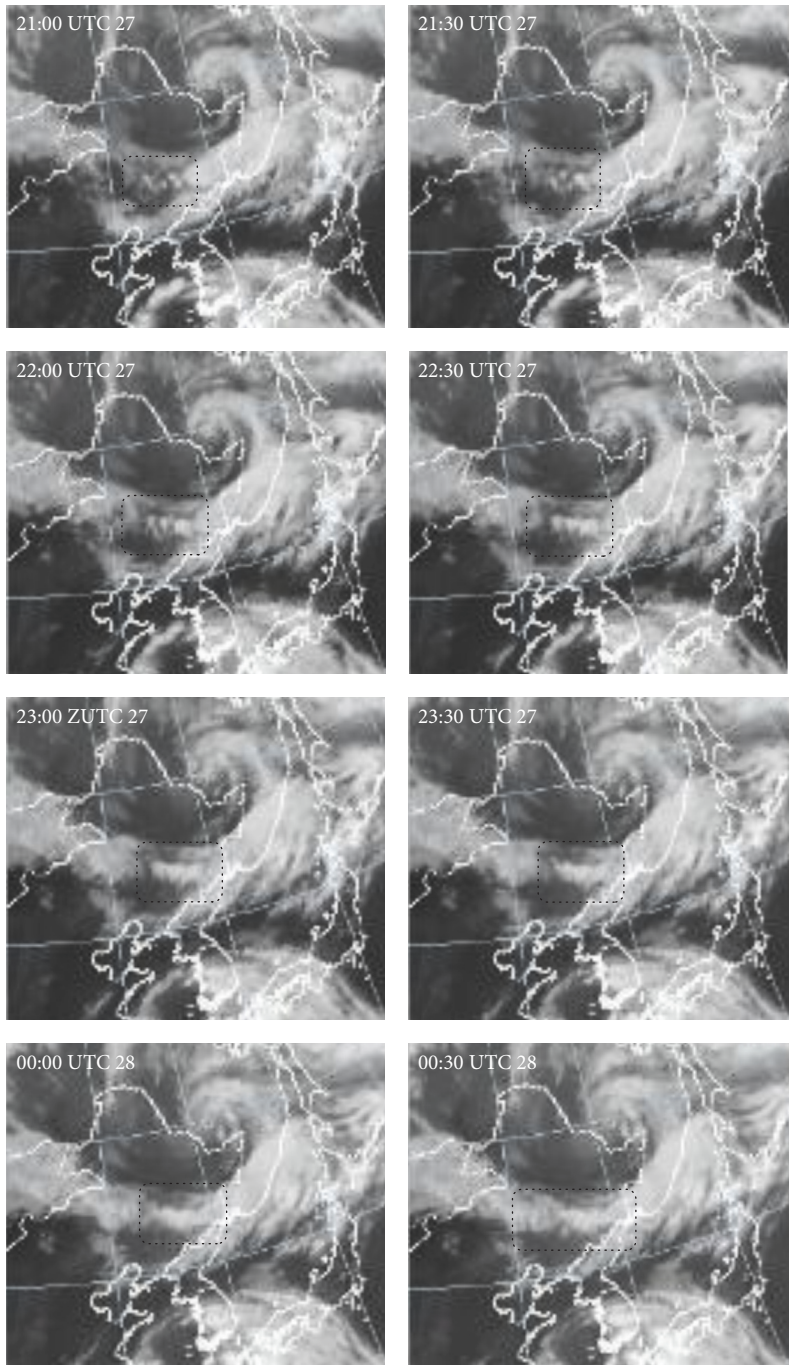

Figure 5: FY2E infrared images of clouds at 30 min intervals from 21:00 on the 27th to 00:30 on the 28th.

reaching 80.5 mm in this area. The C1 and C2 clouds moved eastwards and merged to become C12 clouds, and the −32°C area enlarged, with a west–east extent of 30 km. At 00:00 on the 28th, C12 and C3 clouds moved eastward and merged, forming a meso-α-scale cloud cluster with a closed −32°C contour that extended ~500 km in the east–west direction. The same cloud cluster later moved southeastward, affecting southeastern Jilin. The precipitation center was north of the newly formed clouds, that is, their cold side, where a strong TBB gradient appeared.

3.2. Radar Reflectivity Evolution. The time series of the composite radar reflectivity (Figure 7) shows that the mesoscale system affecting Guanting and Sanjiazi developed in 2 separate stages. From 14:00 to 20:00 on the 27th, the reflectivity had a serrated pattern, indicating that multiple systems moved over the rain area but remained for only a short period. The maximum reflectivity was <35 dBz and the maximum precipitation was 43 mm. From 20:00 to 21:00 on the 27th, the reflectivity was very weak, corresponding to a period with a break in the precipitation. AT 22:00 on the 27th, the

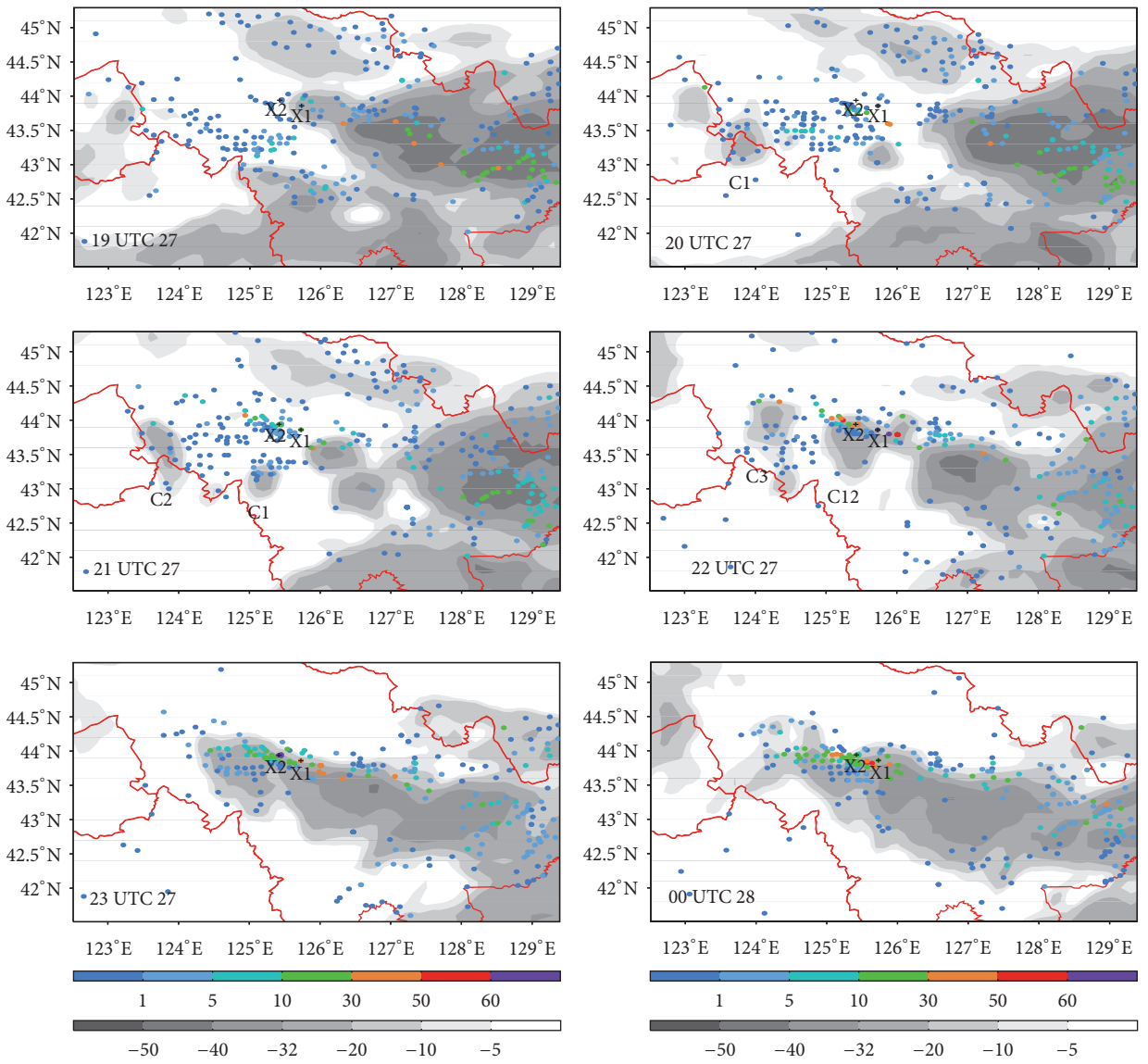

Figure 6: Hourly TBB (shaded, °C) and hourly precipitation (mm) from 19:00 on the 27th to 00:00 on the 28th.

reflectivity rapidly increased to >35 dBz, with a maximum >45 dBz. This strong reflectivity persisted for ~4 h and the maximum hourly precipitation reached 80.5 mm. This indicates that the maximum precipitation intensity corresponded to the maximum reflectivity.

Figures 8(a)–8(f) present the evolution of the radar reflectivity from 13:30 to 18:12 on the 27th. At 13:30, the radar echo belt extended from the west-northwest to east-southeast and contained multiple isolated meso-γ-scale convective cells. The echo belt gradually moved northeastward and affected Guanting and Sanjiazi around 14:30. Afterwards, the strong echo belt moved in an east-southeast direction and isolated convective cells kept forming behind the belt. As shown in Figure 8, the echo configuration was disorganized during this period, implying that isolated convective cells moved over the rain area and caused heavy precipitation there.

Figures 8(g)–8(l) show the evolution of the radar reflectivity at 21:18 on the 27th through 01:06 on the 28th. Compared to the previous stage, the radar echo had a narrow, long belt pattern in this stage. This belt formed at 21:54 on the 27th and became disorganized around 00:06 on the 28th, persisting for ~2 h. In the mature stage (22:48 on the 27th), it had a structure with an inverted "Λ" shape, with the echo junction point corresponding to the heavy rain area at Guanting, where the hourly precipitation reached 80.5 mm.

Figure 9 displays a temporal-longitudinal cross section of the composite radar reflectivity averaged over 43.7°–43.9°N. It clearly shows that the convective cloud cluster that affected the aforementioned rain area mainly formed in the west and then moved eastwards while intensifying. The cloud cluster responsible for the maximum hourly precipitation largely formed and intensified in the rain area. The numerical simulation of this rainfall event also demonstrated this evolution

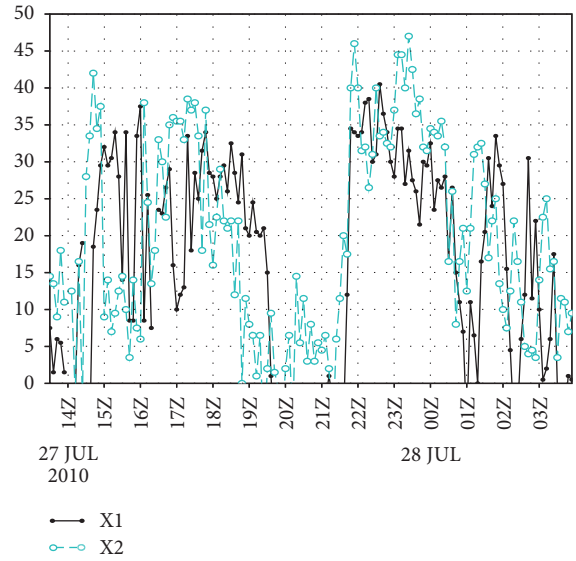

Figure 7: Time series of the composite radar reflectivity from 14:00 on the 27th to 03:00 on the 28th at Guanting (X1) and Sanjiazi (X2).

characteristic. Precipitation in the first stage was caused by the eastward motion of the cold vortex cloud system, whereas in the second stage it could be attributed to the newly formed rain clouds in the rain area after the passage of the main cloud cluster.

4. Precipitation Enhancement

The above analysis reveals that 2 severe precipitation events occurred in areas from Changchun to Yongji, with the hourly precipitation at both Guanting (X1) and Sanjiazi (X2) in the central rain area during the second stage being stronger than that in the first stage. In this section, we analyze the mechanisms for the intensification of the precipitation based on the surface observations and NCEP reanalysis data.

Figure 10 shows 3 h interval surface winds overlain by 1 h precipitation. At 15:00 (Figure 10(b)), westerly and southwesterly winds converged at the surface, generating a maximum of 43 mm of precipitation at 16:00 at Sanjiazi. At 18:00 (Figure 10(c)), the southwesterly winds moved further northwards and prevailed in the rainstorm area, with the convergence caused mainly by the difference of the wind speeds, and the precipitation weakened. The above analysis indicates that the first-stage precipitation is attributable to the convergence of surface westerly and southwesterly winds and the difference of the wind speeds.

At 21:00 on the 27th (Figure 10), easterly winds prevailed from the northeast to east of the rain area, leading to vortex generation to the east. At 00:00 on the 28th (Figure 10(e)), northerly winds prevailed north of the rain area and these were coupled with the southerly winds to the south and easterly winds to the northeast and east of the rain area. This intensified the vortex system and caused its westward shift to the rain area, which explains the reoccurrence of the heavy precipitation at Yongji, where the hourly maximum precipitation reached 80.5 mm. At 03:00 on the 28th (Figure 10(f)), the easterly winds disappeared, the vortex system weakened and moved eastwards, and precipitation ceased.

Figure 11 presents a vertically integrated water vapor flux over 1000–850 hPa and its divergence. From 12:00–18:00 on the 27th, the water vapor flux and area of the flux convergence moved quickly northwards. At 18:00 (Figure 11(b)), the water vapor flux was $>2\,\mathrm{kg\,m^{-1}\,s^{-1}}$ and the flux convergence reached $-0.6\,\mathrm{kg\,m^{-2}\,s^{-1}}$ in the heavy rain area. At 00:00 on the 28th (Figure 11(c)), the heavy rain area was still within the region of the water vapor flux convergence, although the flux had slightly decreased. This result indicates that the water vapor flux and flux divergence were both larger during the second stage than in the first stage of precipitation. In fact, Figure 11(b) clearly shows that at 18:00 on the 27th westerly winds to the north of the rain area gradually turned northerly when huge amounts of water vapor were transported northwards by the southwesterly winds, which enhanced the convergence in the rain area. Apparently, increases in the water vapor supply and the enhanced convergence at the lower levels induced by the northwesterly winds were 2 primary reasons for the intensification of the precipitation in the second stage.

5. Numerical Study of the Abrupt Precipitation Increase

The above analysis reveals that the localized severe precipitation was generated by meso-β- and meso-γ-systems. To explore the mechanisms for the development of these mesoscale systems, numerical sensitivity experiments were conducted to simulate the precipitation process.

The WRF-ARW was used in the study. This model was initialized at 12:00 on the 27th and integrated for 24 h. Different physics schemes were used for comparison. Model physics and parameters are listed in Tables 1 and 2. Initial and boundary conditions were extracted from the global $1^\circ \times 1^\circ$ NCEP reanalysis data, and the ARPS Data Analysis System was used to assimilate the surface observations, sounding data, automatic weather station observations, and TBB to produce the initial conditions for the WRF.

5.1. Model Results and Verification. The model results of the hourly precipitation and composite radar reflectivity from the 5 experiments (Table 1) were verified against observations. It was found that Experiment 1 using the WSM6 scheme could better reproduce the evolution of the precipitation and its influencing systems than the other experiments (Figure 13). Therefore, the subsequent analysis was based on the results of Experiment 1.

The above analysis of the observations reveals that the precipitation was concentrated in 2 periods at Sanjiazi (Figure 12, A1), that is, 16:00–20:00 on the 27th and 21:00 on the 27th to 00:00 on the 28th. Figure 12 displays a comparison of the simulations and observations. Generally, the model realistically simulated the rain belt distribution, especially its quasi-east–west extent. However, the length of the rain belt in the first 6 h integration was shorter than that of the observations, and thus the precipitation at Jilin was not reproduced

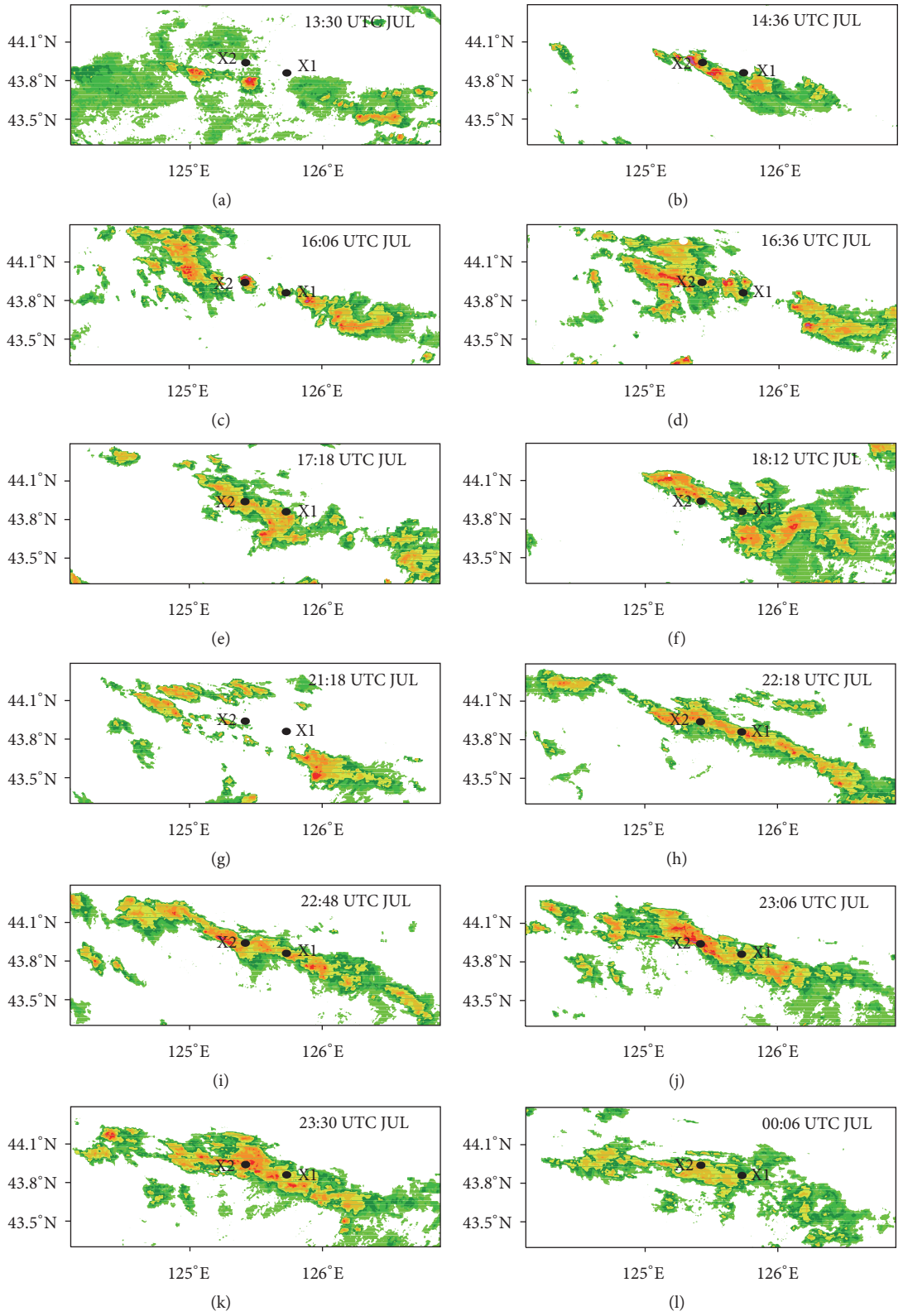

Figure 8: Evolution of the radar reflectivity from 13:30 on the 27th to 00:06 on the 28th (dBz).

Table 1: Experimental design and physics options used in the experiments.

Model	Exp.	Microphysics	Cumulus	Radiation	Land surface	PBL	Surface layer
WRF	1	WSM6	12 km: KF 4 km: off	12 km: RRTM 4 km: Goddard	Unified Noah land surface	YSU	Monin-Obukhov
WRF	2	Lin	Ditto	Ditto	Ditto	Ditto	Ditto
WRF	3	Thompson	Ditto	Ditto	Ditto	Ditto	Ditto
WRF	4	Milbrandt	Ditto	Ditto	Ditto	Ditto	Ditto
WRF	5	WDM6	Ditto	Ditto	Ditto	Ditto	Ditto

Table 2: Model parameters.

Horizontal resolution (km)	Model domain center	Horizontal grid size	Number of vertical levels
12	42°N, 122°E	271 × 256	53
4	42°N, 122°E	319 × 301	53

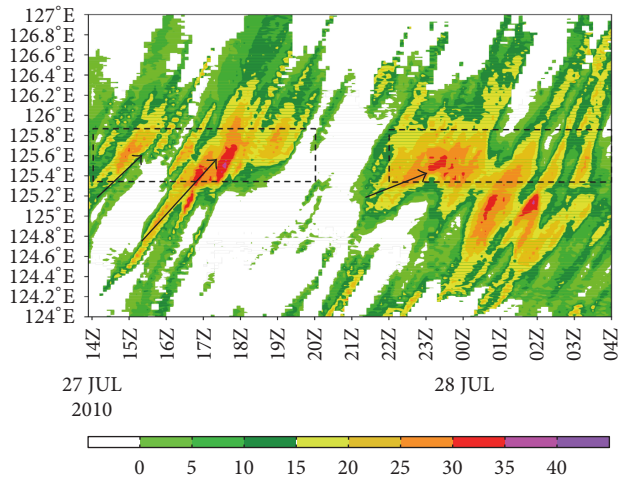

Figure 9: Time-longitude cross section of the composite radar reflectivity averaged over 43.7°–43.9°N (dBz).

by the model. The simulated precipitation in the first stage over A1 was weaker than the observations and little more southerly than the actual location. The observations indicated that sparse centers of hourly precipitation of >20 mm first appeared at 17:00, but such centers were south of the actual location in the simulation until after 19:00. Observations indicated that the precipitation over A1 abruptly increased at 23:00 on the 27th with an hourly precipitation > 50 mm at the rain center, whereas a precipitation center south of the observed center with an hourly precipitation > 40 mm was simulated by the WRF. However, the simulation and observations were generally consistent over A2.

The above analysis indicates that the model could reproduce the evolution of the precipitation process, although there were certain differences between the simulation and observations over A1 in the initial several hours of the integration. In addition, the model satisfactorily reproduced the abrupt increase in the precipitation over A1. Therefore, in the following section, we explore the thermodynamic mechanisms for that abrupt increase based on the model results.

5.2. Three-Dimensional Structure. The above analysis shows that the precipitation in the second stage over A1 started intensifying at 21:00 on the 27th. We used the vertical-latitudinal cross sections of the system in various stages of development in Figure 13 to analyze the convective system structure in the second stage. At 21:00 (Figure 13(a)), the convective cell developed from the lower levels and the main body of the cell was below the 700 hPa level, with an ascending flow prevalent within the convective system. At 21:50 (Figure 13(b)), the convective cell developed rapidly and extended vertically to the 350 hPa level, with a strong ascent within. The precipitation increased, with the 10 min rainfall > 5 mm. At 22:20 (Figure 13(c)), the convective cell reached 250 hPa and its convection strengthened, with its center at 400–600 hPa. The 10 min precipitation reached 10 mm. In contrast with the previous period, descending motions appeared inside the convective system, and a cold center developed near the surface layer to the south of the convective cell. At 22:40 (Figure 13(d)), new convective systems began to form in the surface layer near the cold center, as shown in Figure 13(d), while the convective cell weakened in concert with the descending motions, as did the 10 min precipitation. Simultaneously, another cold center appeared to the south of the convective cell. The temperature decline was more obvious compared to that in the previous period. At 23:10 (Figure 13(e)), a convective cell corresponding to the previous cold center developed and the vertical depth of the severe convection increased, extending from 300 to 750 hPa. A strong ascent prevailed inside the convective system, while a descending motion appeared to the south of the system. The 10 min precipitation reached 15 mm. Another cold center formed immediately south of the precipitation center, and the temperature decline was even more obvious than that in the previous cold center. New convective cells formed concurrently at low levels, coincident with the cold center. At 23:30 (Figure 13(f)), the previously formed convective cell developed further while the convective system to its north weakened and new cold centers appeared to its south.

The above analysis suggests that newly developed convective cells correspond to cold centers within the surface convergence line. The stronger the cold center, the more severe the convective system and the heavier the precipitation. The convective cell in its mature stage weakened rapidly and eventually disappeared due to the descent induced by the heavy precipitation drag and was replaced by newly formed

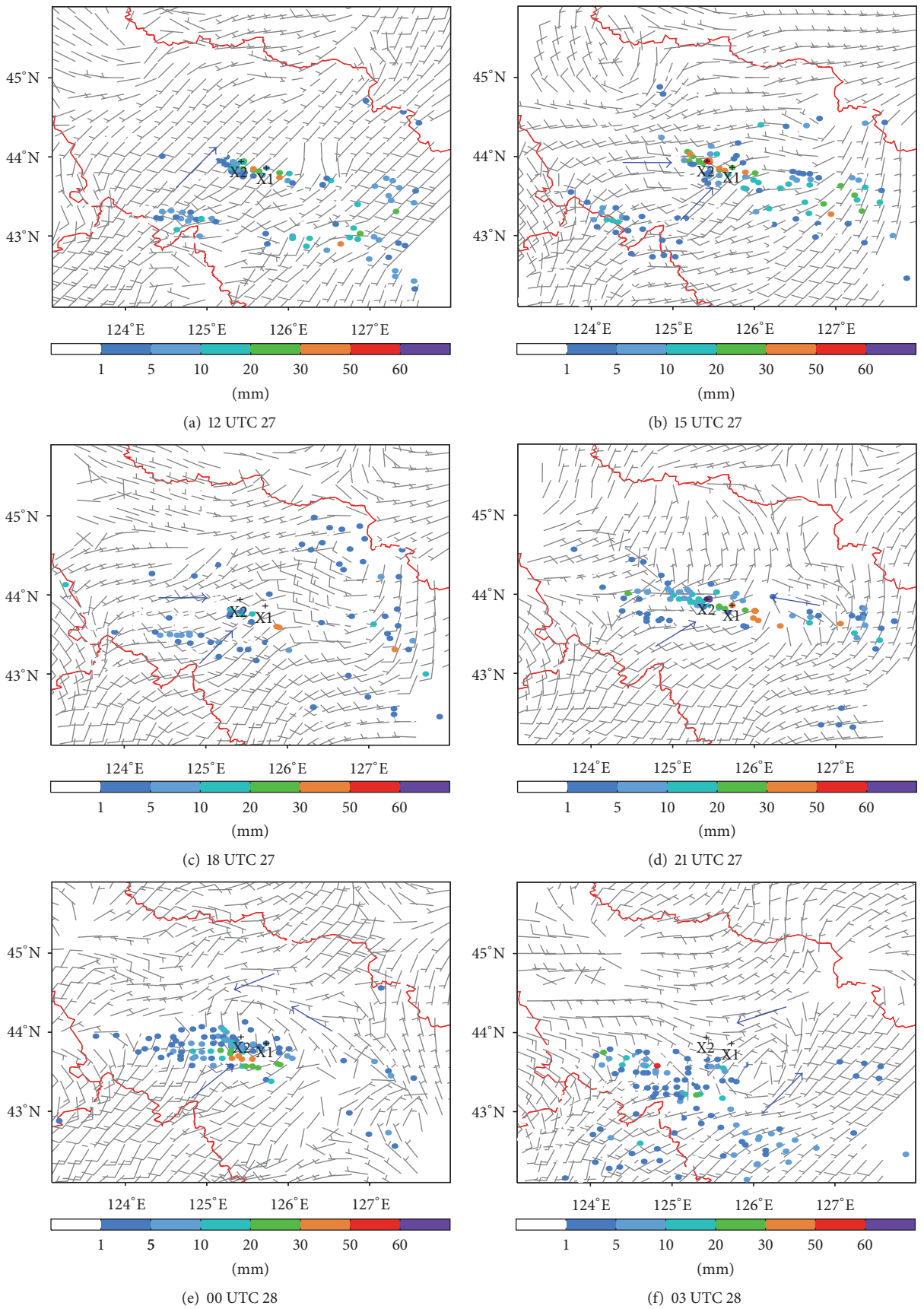

(a) 12 UTC 27

(b) 15 UTC 27

(c) 18 UTC 27

(d) 21 UTC 27

(e) 00 UTC 28

(f) 03 UTC 28

Figure 10: Surface winds at 3-hour intervals (full barb for 4 m s^{-1}) and 1 h precipitation (colored dots) from 12:00 on the 27th to 03:00 on the 28th. Blue arrows indicate the prevailing flow.

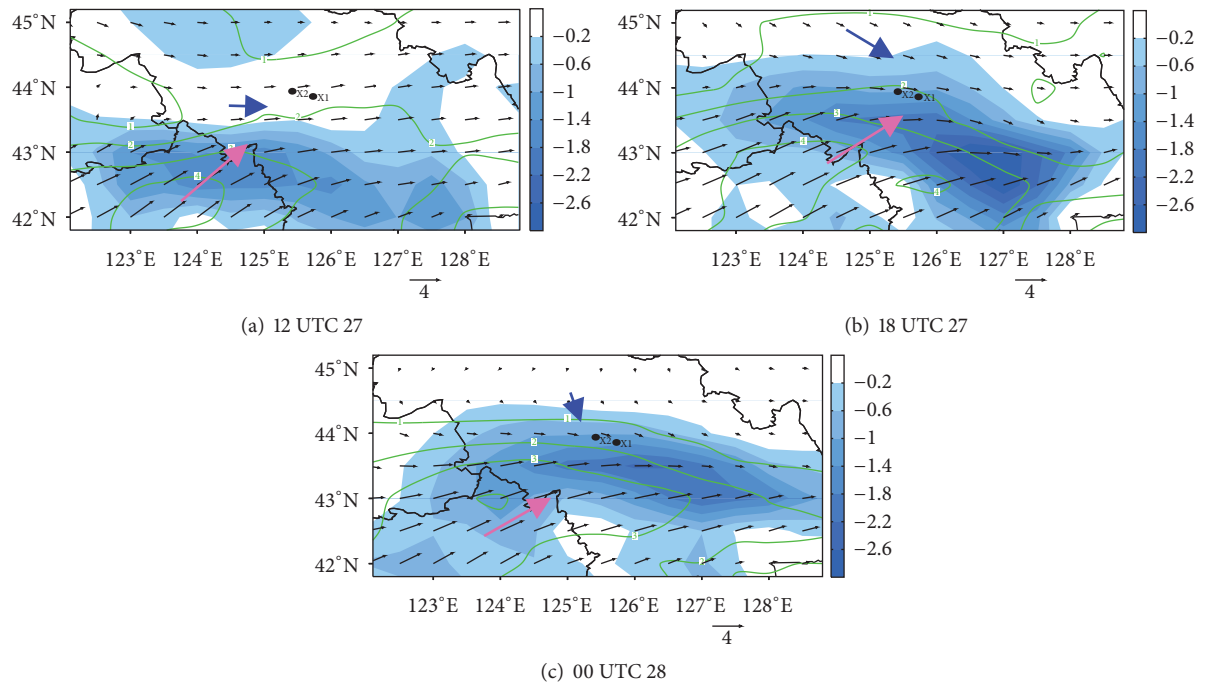

(a) 12 UTC 27

(b) 18 UTC 27

(c) 00 UTC 28

Figure 11: Atmospheric water vapor fluxes, with flux vectors integrated over 1000–850 hPa (contours, kg m^{-1} s^{-1}), and the water vapor flux divergence (shaded, kg m^{-2} s^{-1}). Rose arrows indicate a warm moist flow, and blue arrows indicate a cold flow.

convective cells. Cold centers near the surface often appeared on the warmer side of the heavy precipitation center, corresponding to newly formed convective cells. Therefore, it is important to monitor the development and evolution of cold centers in the surface layer, which is critical in forecasting new convective cells. This is because the intensity of the cold center affects the strength of the convective cell and subsequent precipitation.

5.3. Precipitation Enhancement. Figure 14 shows the latitude-time cross sections of the system evolution along 125.4°E at 00:00 on the 27th to 01:00 on the 28th. During the first period of precipitation (17:00–20:00 on the 27th), southwesterly and northwesterly winds converged at 950 hPa, while westerly winds prevailed at 850 hPa. In the second period of precipitation (21:00 on the 27th to 01:00 on the 28th), the northwesterly winds at 950 hPa gradually turned northeasterly at 21:30, which converged with the southwesterly winds to their south over area A1, producing a convergence line that persisted continuously from 21:30 to 23:00. During the same period, southwesterly winds prevailed at 850 hPa with increased speeds. Precipitation occurred within 20 km north of the convergence line. After 23:00, the convergence line moved rapidly southward, and there was no more precipitation over area A1.

The above analysis indicates that mid- and low-level winds changed substantially during the 2 precipitation periods; that is, the low-level northwesterly winds gradually turned northeasterly, while westerly winds at mid-levels changed to southwesterly winds with increased speeds. These changes led to heavier precipitation in the second period relative to that in the first period. Next, we investigated the causes for these wind field changes. Mid- and low-level streamlines and their topography are plotted in Figure 15, from which it can be observed that the severe precipitation area (A1) was at the base of the U-shape topography west of Changbai Mountain. At 18:00 on the 27th, this area was under the control of northwesterly winds, which converged with the southwesterly winds to their south and generated the first-period precipitation (Figure 15(a)). As the cold vortex gradually moved southeast, it was blocked by the northeast–southwest-oriented Changbai Mountain. Thus, the northwesterly winds turned northerly and northeasterly (Figure 15(b)). Similarly, the southwesterly winds to the south of the mountain were forced to flow around it, strengthening the southwesterlies to the west of the mountain. The southwesterly and northeasterly winds converged at the base of the U-shape topography, producing heavy precipitation there. Subsequently, the northeasterly winds extended further westwards (Figures 15(c) and 15(d)), followed by the westward extension of the low-level convergence line, which continuously triggered new convection. This produced the second period of precipitation. From the streamlines at 850 hPa (figure not shown), it is clear that the southwesterly winds were blocked by Changbai Mountain and were forced to flow around it. Wind speeds increased to the southwest of the mountain, and the southwesterly winds at 850 hPa reached a little more northerly than those in the lower levels because the topography is relatively low at the U-shaped bottom. As a result, cold northeasterly winds prevailed at the surface, warm and moist southwesterly winds dominated the middle to lower levels, and cold northwesterlies prevailed at the middle to higher levels. Under such a configuration, the atmospheric stratification was extremely

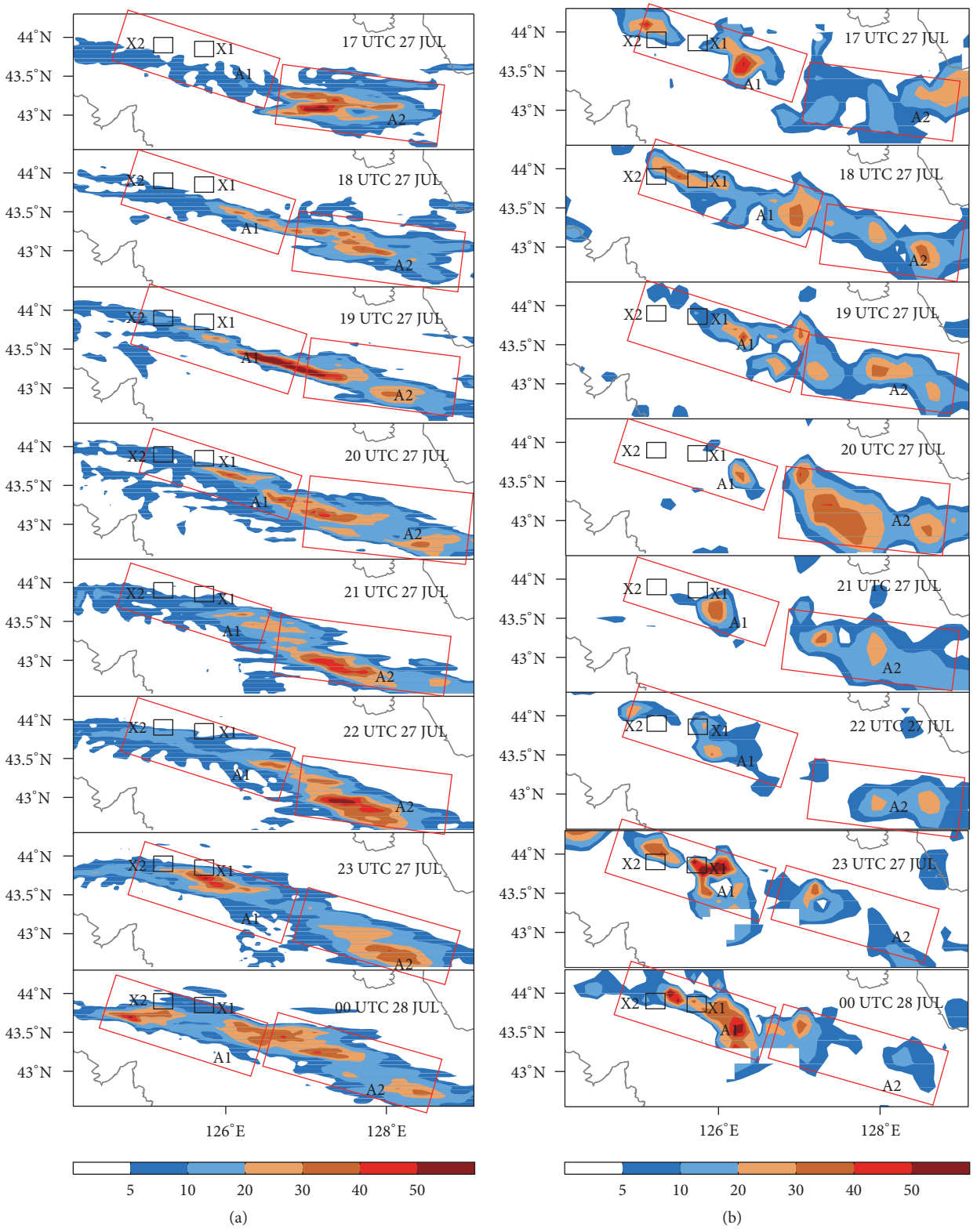

Figure 12: Simulated (a) and observed (b) hourly precipitation (unit: mm). Corresponding time shown in upper left corner of each panel. The period is from 16:00 on the 27th to 00:00 on the 28th. The rectangles in the plots indicate the 2 areas of rainfall (the left is A1 and the right is A2). The directions of the rectangles are roughly consistent with those of the rain belts.

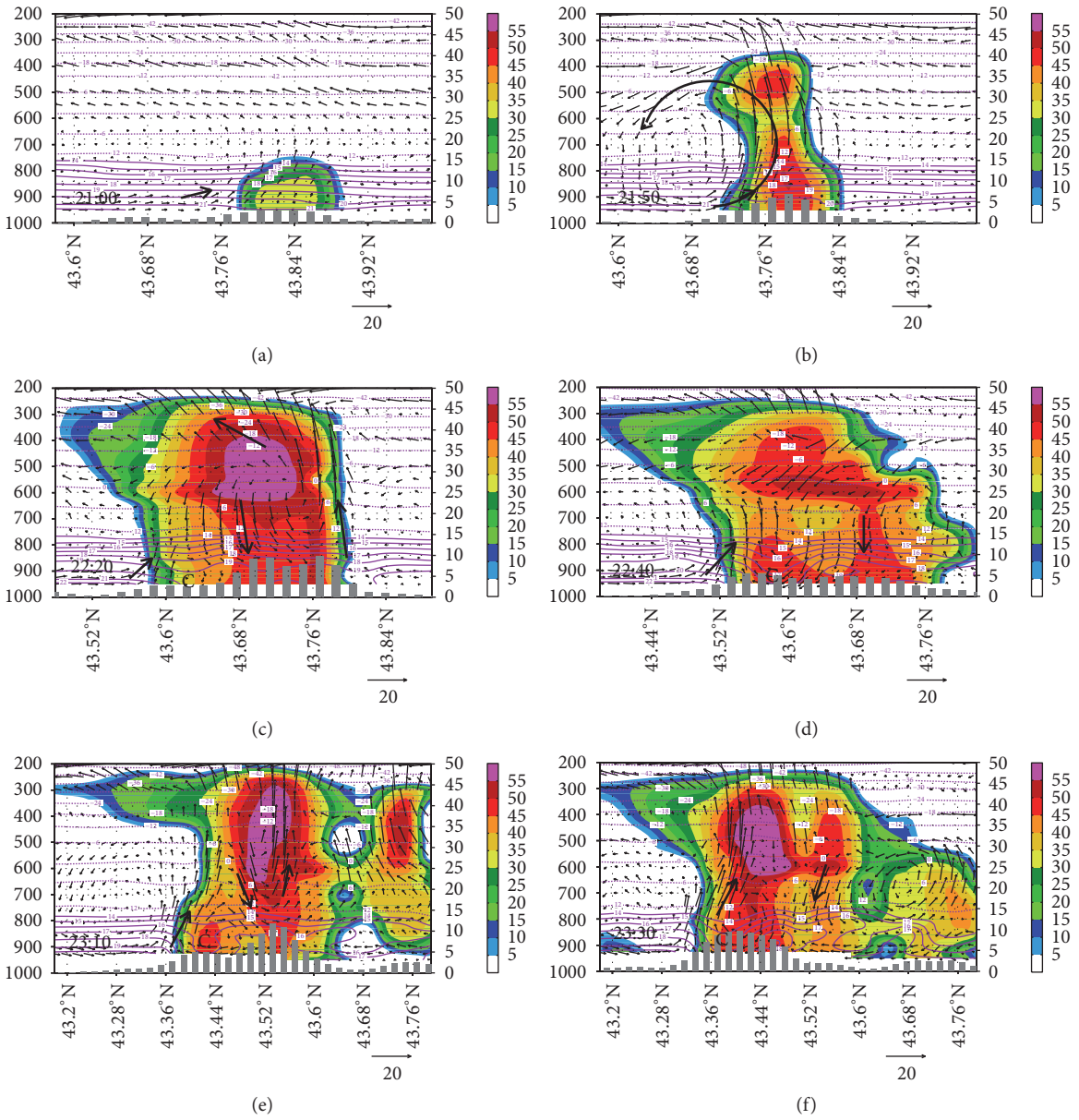

Figure 13: Vertical-latitudinal cross sections of the convective cell causing the second severe precipitation event in various stages of the development of the reflectivity (shaded, dBz), 10 min precipitation (histogram at the panel base, mm), temperature (isolines, ˚C), and wind (vectors, created by combining v with $w * 10$). "C" indicates the cold center.

unstable at the U-shaped area, which was favorable for the development of severe convection. The evolution of the precipitation (figure not shown) showed heavy precipitation north of the surface convergence line and south of the convergence line at mid-levels. The maximum precipitation occurred when there were low-level northeasterlies and southwesterlies that encountered each other. As the cold vortex continued to move southeastwards, the cold air mass and precipitation moved south, so precipitation over area A1 weakened.

The above analysis suggests that the turning of the northwesterly to northeasterly winds was a critical reason for the occurrence of precipitation during the second period, which is consistent with the evolution of the observed surface winds. This implies that the changes in the low-level circulation could provide helpful information for accurate precipitation forecasting.

To further explain the relationship between the precipitation increase and the mid- to low-level wind field changes, we compared the meridional wind speed at the time of the precipitation intensification (23:00 on the 27th) with that of the previous hour (22:00). Figure 16 shows a vertical cross section of the meridional wind difference between those 2 hours along 125˚E. The area of a large southerly wind difference was between 700 and 900 hPa and tilted northward with height. The area of a large northerly wind difference was

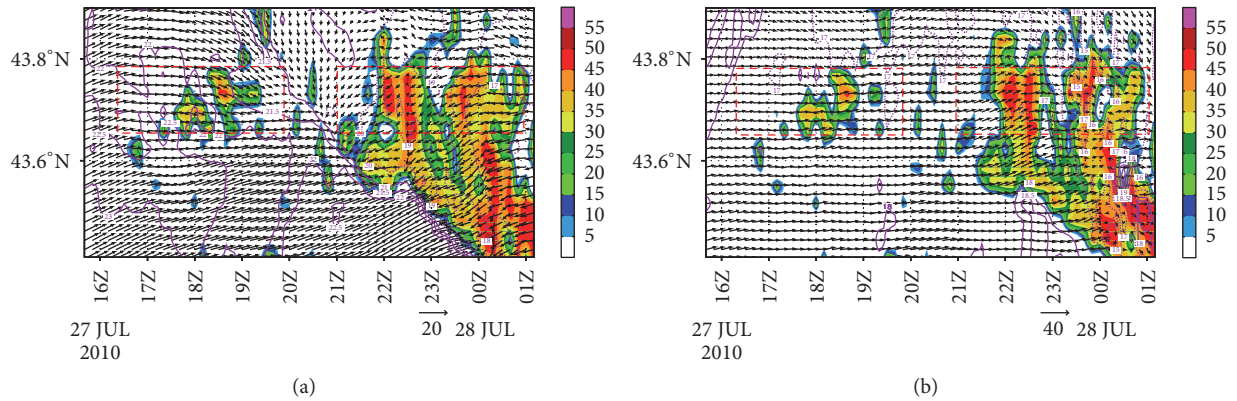

Figure 14: Latitude-time cross sections of the system evolution along 125.4°E for the reflectivity (shaded, dBz), temperature (isolines, °C), and horizontal winds (vectors, m s^{-1}). The rectangles indicate the 2 periods of heavy rainfall at A1: (a) 950 hPa and (b) 850 hPa. The time interval is 10 minutes.

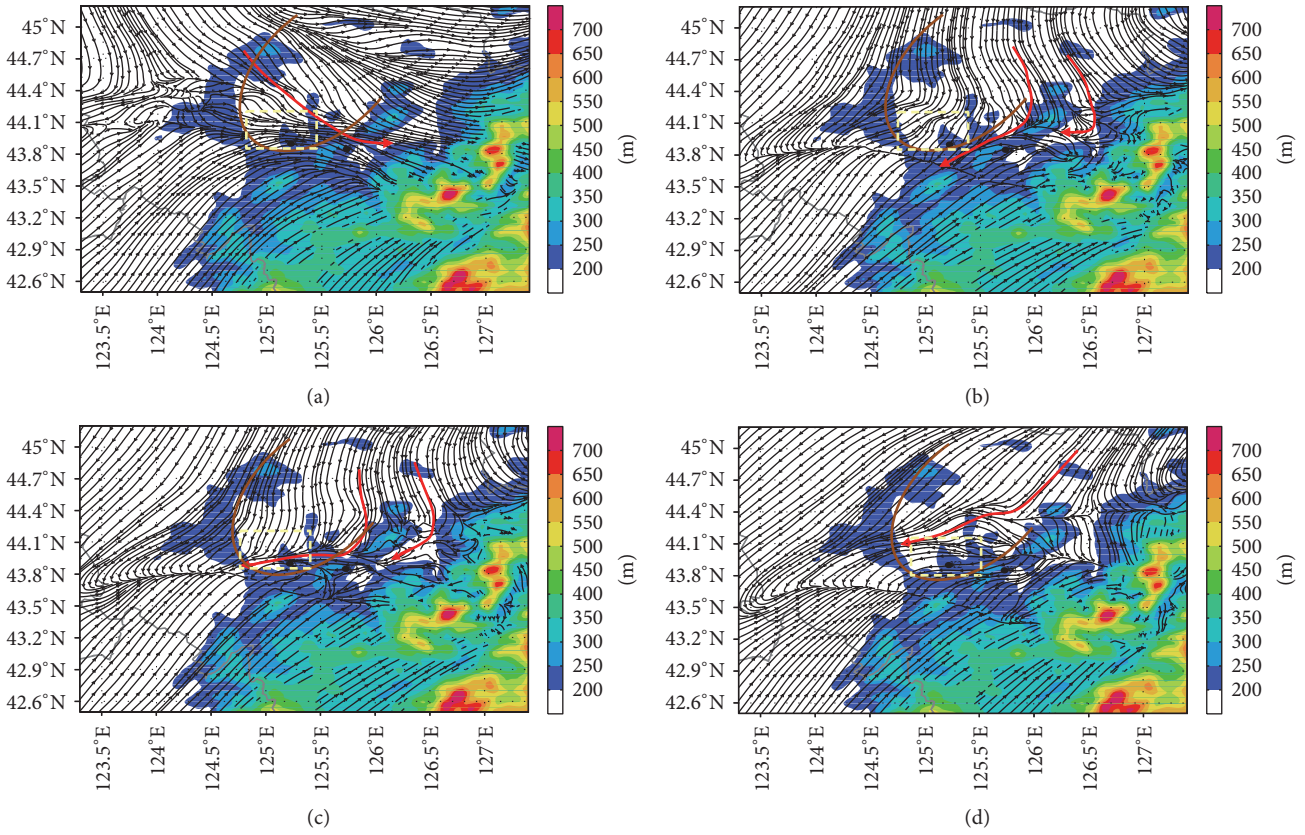

Figure 15: Streamlines at 950 hPa and the topography (shading indicates the topography elevation, unit: m; the red arrows indicate the northerly flow direction, the brown line represents the U-shaped topography, and the yellow rectangle indicates heavy rain in area A1): (a) 18:00 on the 27th, (b) 21:50 on the 27th, (c) 22:30 on the 27th, and (d) 00:00 on the 28th.

near the surface. Strong vertical velocity changes appeared near 500 hPa, and there was a precipitation maximum where the strong northerly wind change near the surface coincided with the strong southerly wind change at the upper levels (dashed rectangle in Figure 16). Figure 16 also shows that the low-level northerly winds intensified and wedged under the warm, moist southwesterly winds, lifting the warm, moist air mass and triggering deep convection.

6. Conclusions and Discussion

We performed a comparative study between 2 completely different episodes of rainfall within a local severe precipitation event caused by a cold vortex over Northeast China. The event was divided into 2 stages. From 14:00 to 20:00 on the 27th, there was a severe rainfall over Yongji, and the central rain area extended from Sanjiazi to Guanting. Two hours

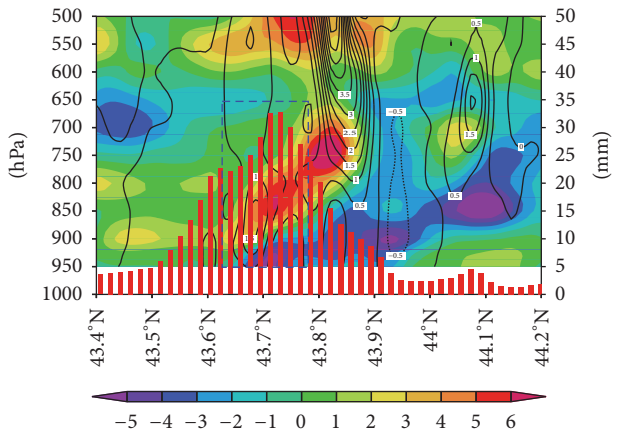

Figure 16: Vertical cross section of the differences in the meridional velocity (shaded, m s^{-1}) and vertical velocity (isolines, m s^{-1}) between 23:00 and 22:00 27 July 2010 along 125°E, and the 1 h precipitation of 22:00-23:00 (red histogram, mm) (the dashed rectangle indicates an area of strong convergence between the southerly and northerly winds).

later, there was another heavy precipitation process almost in the same area with a greater intensity than the previous one. The precipitation in the first period was attributed to the convergence of the northwesterly winds at the rear of the cold vortex with southwesterly winds that reached Northeast China. At low levels, the isolated convective clouds aligned with the shear line and moved northeast, generating heavy precipitation when they reached the rainfall area. In the second precipitation stage, the bottom part of the cold vortex was controlled by northeasterly winds, which strongly converged with southwesterly winds and led to the heavy rains. Compared with the first period of the precipitation event, the convective clouds that caused precipitation in the second period developed first in the heavy rainstorm area and gradually formed a narrow, elongated linear structure. In the mature stage, the cloud structure had an inverted Λ configuration, and the heavy precipitation occurred at the top of the Λ.

This study used the dense surface observations, infrared satellite and radar measurements, and NCEP reanalysis data to perform the comparative analysis of the 2 consecutive precipitation events at Yongji from 27 to 28 July 2010. The WRF model was used to simulate the events for investigating the relevant dynamic and thermodynamic mechanisms. The major results are as follows.

(1) The numerical results indicate that the rainstorm's center was located at the bottom of the U-shaped topography. When the northerly winds at low levels entered this topographic area, the airflow was blocked. As Changbai Mountain is to the east of that area, the blocked air was deflected westwards, where the topography was relatively low. The northeasterly winds prevailed, with the result that the low-level cold air mass retreated westwards along the convergence line. The southwesterly winds to the south prevailed around Changbai Mountain as a result of the blocking effect of the mountain, and thus the wind speeds increased west of that mountain. The southwesterly winds converged with the northeasterlies to form an east–west convergence line, along which new convection was continuously triggered.

(2) The newly generated convective cells were collocated with cold centers along the surface convergence line. The stronger the cold center, the more intense the convective system and the heavier the precipitation. Descending motions developed within the mature convective cells because of the drag induced by the heavy precipitation, which led to a rapid weakening and disappearance of those cells.

(3) Cold centers at the surface often appeared on the warmer side of the severe precipitation center, corresponding to newly formed convective cells. Therefore, it is important to monitor the development and evolution of cold centers in the surface layer, as this is critically important in forecasting the formation of new convective cells. The intensity of the cold center affects the strengths of the convective cells and subsequent precipitation.

(4) Convective weather events against the background of a northeast cold vortex often develop when northwesterly winds prevail at the middle to upper levels. These events are characterized by small scale, abrupt occurrences, and complicated weather phenomena, have a powerful destructive potential, and are difficult to predict in operational weather forecasts. The results of the present study indicate that the precipitation was not distributed evenly along the surface convergence line. Instead, it was closely associated with the cold centers along that line. The intensity of the cold center directly affected the intensity of the precipitation. Local terrain features and the direction of motion of the airflows were critical in triggering convection. This research provides a valuable reference for practical weather forecasting.

The present study focused only on a single event and addressed the preliminary terrain and airflow impacts on the convection initiation. More studies are necessary for further revealing the mechanisms of disastrous weather events.

Conflicts of Interest

The authors declare that there are no conflicts of interest regarding the publication of this article.

Acknowledgments

This work was jointly supported by the National Natural Science Foundation of China under Grants 41075048 and 91437221 and the R&D Special Fund for Public Welfare Industry (Meteorology) of the Ministry of Finance and Ministry of Science and Technology under Grants GYHY201006006, GYHY201306004, and GYHY201506002. The gridded radar data used were produced by the weather radar 3D mosaic

system developed by Dr. Hongyan Wang of the Chinese Academy of Meteorological Sciences.

References

[1] L. Gimeno, R. M. Trigo, P. Ribera, and J. A. García, "Editorial: Special issue on cut-off low systems (COL)," *Meteorology and Atmospheric Physics*, vol. 96, no. 1-2, pp. 1-2, 2007.

[2] E. Palmen and C. Newton, *Atmospheric Circulation System: Their Structure and Physical Interpretation*, Academic Press, 1969.

[3] L. Sun, X. Zheng, and Q. Wang, "The climatological characteristics of Northeast Vortex in China," *Quarterly Journal of Applied Meteorology*, vol. 5, no. 3, pp. 297–303, 1994 (Chinese).

[4] H. Yang, G. Feng, B. Shen, and R. Zhi, "The quantitative research on cold vortex in summer over Northeast China," *Chinese Journal of Atmospheric Sciences*, vol. 36, no. 3, pp. 487–494, 2012 (Chinese).

[5] D. Wang, S. Zhong, Y. Liu et al., "Advances in the study of rainstorm in Northeast China," *Advances in Earth Science*, vol. 22, no. 6, pp. 549–560, 2007.

[6] Z. Xie, C. Bueh, L. Ji, and S. Sun, "The Cold Vortex Circulation over Northeastern China and Regional Rainstorm Events," *Atmospheric and Oceanic Science Letters*, vol. 5, no. 2, pp. 134–139, 2012.

[7] J. He, Z. Wu, Z. Jiang, C. Miao, and G. Han, "'Climate effect' of the northeast cold vortex and its influences on Meiyu," *Chinese Science Bulletin*, vol. 52, no. 5, pp. 671–679, 2007.

[8] C. Miao, Z. Wu, J. He, and Y. Chi, "The anomalous features of the northeast cold vortex during the first flood period in the last 50 years and its correlation with rainfall in South China," *Chinese Journal of Atmospheric Sciences*, vol. 30, no. 6, pp. 1249–1256, 2006 (Chinese).

[9] S. Matsumoto, K. Ninomiya, R. Hasegawa, and Y. Miki, "The Structure and the Role of a Subsynoptic-Scale Cold Vortex on the Heavy Precipitation," *Journal of the Meteorological Society of Japan. Ser. II*, vol. 60, no. 1, pp. 339–354, 1982.

[10] L. Sun, Q. Wang, and X. Tang, "A composite diagnostic analysis of cold vortex of storm-rainfall and non-storm rainfall types," *Meteorological Monthly*, vol. 21, no. 3, pp. 7–10, 1995.

[11] X. Liu and X. Guo, "Analysis and numerical simulation research on severe surface wind formation mechanism and structural characteristics of a squall line case," *Chinese Journal of Atmospheric Sciences*, vol. 36, no. 6, pp. 1150–1164, 2012.

[12] W. Xu, D. Lü, L. Shen, F. Liu, and H. Wang, "Characteristic condition analysis for forecasting convective weather of upper cold falling vortex," *Scientia Meteorologica Sinica*, vol. 29, no. 5, pp. 618–624, 2009.

[13] J. Dai, L. Tao, Y. Ding, Y. Wang, and L. Chen, "Case analysis of a large hail-producing severe supercell ahead of a squall line," *Acta Meteorologica Sinica*, vol. 70, no. 4, pp. 609–627, 2012.

[14] Y. Hsieh, "An investigation of a selected cold vortex over north America," *Journal of the Atmospheric Science*, vol. 6, pp. 401–410, 1949.

[15] M. Feng, Y. Zhong, Y. Wang, X. Jiao, and B. Xu, "Comparative Analysis on Characteristics of Two Lightning Processes under Northeast Cold Vortex," *Journal of Catastrophology*, vol. 25, no. 4, pp. 54–58, 2010.

[16] Y. Zhang, S. Niu, S. Xi, J. Liang, P. Song, and H. Zhou, "Analysis on Characteristic of Severe Convective Weather in Henan in the Situation of Northeast Vortex and the Back of Trough," *Torrential Rain and Disasters*, vol. 30, no. 3, pp. 193–201, 2011.

[17] Z. Xie and C. Bueh, "Different types of cold vortex circulations over northeast China and their weather impacts," *Monthly Weather Review*, vol. 143, no. 3, pp. 845–863, 2015.

[18] Z. Xie and C. Bueh, "Cold vortex events over Northeast China associated with the Yakutsk-Okhotsk blocking," *International Journal of Climatology*, vol. 37, no. 1, pp. 381–398, 2017.

[19] L. Chen, L. Zhang, and S. Yang, "Environmental conditions of continual rainstorm caused by northeast cold vortex," *Journal of Meteorology and Environment*, vol. 22, no. 6, pp. 1–5, 2006.

[20] D. Li, C. Wang, and W. Liu, "Numerical simulation on local storm caused by northeast cold vortex," *Journal of Meteorology and Environment*, vol. 25, no. 6, pp. 29–33, 2009.

[21] W. Jin, Y. Qu, and L. An, "Analysis on the Tornado Weather Process Induced by a Super-cell," *Meteorological Monthly*, vol. 35, no. 3, pp. 36–43, 2009.

[22] J. Sun, K. Dai, and L. Fan, "Analysis and Forecasting Technology on the Heavy Rainfall Processes in the Northeast China During July to August 2010," *Meteorological Monthly*, vol. 37, no. 7, pp. 785–794, 2011.

[23] B. Wang and Y. Zhang, "Analysis of a Large-scale Severe Precipitation Event in Jilin Province From 27 to 29 July 2010," *Torrential Rain and Disasters*, vol. 30, no. 1, pp. 36–43, 2011.